International Journal of
INTELLIGENT SYSTEMS AND APPLICATIONS IN ENGINEERING
ISSN:2147-6799 www.ijisae.org Original Research Paper

An Automatic Multi-Variate Multi-Class Feature Extraction, Ranking Based Joint Probabilistic Segmentation and Classification Framework for Multi-Class Liver Tumor Detection

N. Nanda Prakash[1*], V. Rajesh[2], Sandeep Dwarkanath Pande[3], Syed Inthiyaz[4], Sk Hasane Ahammad[5], Dharmesh Dhabliya[6], Rahul Joshi[7]

Submitted: 07/02/2024 **Revised**: 15/03/2024 **Accepted**: 21/03/2024

Abstract: Automatic multivariate and multi-class tumor detection plays a crucial role in the diagnosis and treatment of large heterogeneous liver databases. However, existing liver segmentation models often encounter challenges such as multi-modal tumor detection, detecting tumors with varying shapes, liver over-segmentation, and difficulty in identifying tumors with different orientations and shapes. Moreover, the presence of noise in excessively segmented border regions can further complicate the segmentation and classification process, leading to inconsistent and inaccurate results. In this work, we propose novel approaches for multivariate liver filtering, multivariate feature extraction, and ranking. We employ efficient multivariate segmentation-based classification methods to enhance the overall detection of multi-modal tumors on large databases. The proposed Multi-variate Liver and Tumor Segmentation and Classification (MCMVLTSC) model efficiently classifies key tumor segmented regions with a high true positive rate and runtime efficiency (ms). To evaluate the performance of our proposed MCMVLTSC model compared to existing models, we utilize various statistical measures on diverse liver imaging databases. Experimental results demonstrate that the proposed model outperforms conventional models in terms of different statistical classification metrics and runtime efficiency.

Keywords: *Multi-variate Liver filtering, Multi-class Liver segmentation, deep learning classifiers*

1. Introduction

Liver tumours are formed due to the uncontrolled growth of Liver cells, leading to the development of a mass. As per estimates, there were around 297,000 cases of CNS cancer reported worldwide in 2020, making it the 17th most common form of cancer. However, the high fatality rate of CNS tumours has made it the 12th most frequent cause of cancer-related deaths globally. The rarity and diverse nature of CNS tumours make it challenging to conduct an epidemiological analysis. Various factors like genetic predisposition, exposure to environmental toxins, and medical conditions such as asthma and eczema can contribute to the formation of Liver tumours. The growth of a tumour in the Liver can cause obstruction of fluid flow and increased pressure within the skull, leading to potential damage to Liver tissues and severe neurological issues. A benign tumour is less harmful and can be treated successfully, while a malignant tumour is more dangerous due to its ability to grow and spread to other regions like the spinal cord. Medical imaging techniques such as CT and MRI scans are frequently employed to identify Liver tumors. However, these methods may not always provide precise information regarding the tumor's size and location. It is noteworthy that cancerous Liver tumors usually originate from secondary tumors and can result in various symptoms depending on their position and size within the Liver. The Liver is made up of three different types of tissues: grey matter, white matter, and cerebrospinal fluid as shown in figure 1.

[1]*Department of ECE, Koneru Lakshmaiah Education Foundation, Vaddeswaram, Guntur, 522302, India.*
Email: nandaprakashnelaturi@gmail.com,
[2]*Department of ECE, Koneru Lakshmaiah Education Foundation, Vaddeswaram, Guntur, 522302, India.*
Email: rajesh4444@kluniversity.in,
[3]*School of Computer Engineering, MIT Academy of Engineering, Alandi, Pune. Dist: Pune, Maharashtra–412105, India.*
Email: sandeep7887pande@gmail.com,
[4]*Department of ECE, Koneru Lakshmaiah Education Foundation, Vaddeswaram, Guntur, 522302, India.*
Email: syedinthiyaz@kluniversity.in,
[5]*Department of ECE, Koneru Lakshmaiah Education Foundation, Vaddeswaram, Guntur, 522302, India.*
Email: ahammadklu@gmail.com
[6]*Professor, Department of Information Technology, Vishwakarma Institute of Information Technology, Pune, Maharashtra, India.*
Email: dharmesh.dhabliya@viit.ac.in,
[7]*Associate Professor, Computer Science and Engineering, Symbiosis Institute of Technology, Pune, Symbiosis International (Deemed University), Pune - 412115, India.*
Email: rahulj@sitpune.edu.in

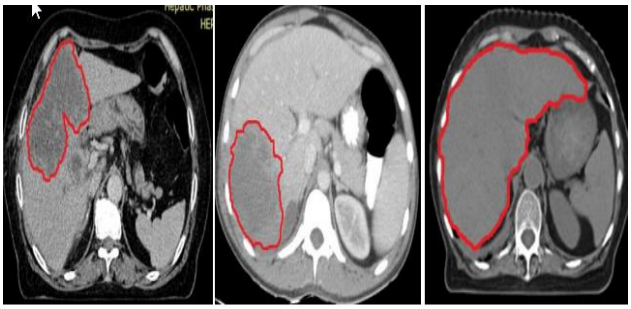

Fig. 1. Different shapes and orientation of liver tumors in large databases

The emergence of a Liver tumor introduces a new tissue class that can be challenging to differentiate from normal Liver tissue due to overlapping intensities. Despite being the most commonly used medical imaging tools for detecting Liver tumors, CT and MRI scans may not always yield accurate results regarding the tumor's location and size. When it comes to diagnosing and treating Liver tumours, non-invasive CT imaging is a commonly used technique. This involves the use of X-ray beams to produce 2D images of the patient's head from various angles, which are then used to create a 3D tomographic image. However, CT imaging has been found to cause damage to the body due to the ionising radiation and dyes used. As a result, MRI has become the preferred method for capturing images of the Liver. It is highly regarded by both doctors and patients alike. Magnetic Resonance Imaging (MRI) is a medical technique that utilizes the magnetic properties of hydrogen nuclei, which are abundant in the human body, to examine glioma tumors. At the outset, the scans included data from both pre- and post-operative periods, but in 2017, the post-operative scans were removed from the dataset [1]. Accurate characterization of grayscale regions is dependent on essential features that indicate a break or change in pattern. The tone of a texture is determined by pixel intensity properties, and the structure depends on the spatial relationship between pixels. Statistical features are critical for precise characterization of grayscale regions [2]. In order to segment Liver tumors, researchers have identified the atlas based segmentation technique as highly effective. This method involves the creation of an atlas or reference table that utilizes data on the size, shape, and characteristics of various organs. Like other correlation-based techniques, it performs both classification and segmentation simultaneously. A study conducted by experts [3] utilized this technique by first aligning the image of a tumorous Liver with a healthy Liver atlas image to detect abnormal Liver tissues. This was followed by the identification of various statistical features, such as variance, mean, median, kurtosis, and other higher-order statistics features, which were obtained from the values of pixels. The process of identifying edema involved the use of imaging technology, specifically T2 images. However, the GMM model has improved efficiency by eliminating the need for manual seed point selection. Model-based techniques leverage the repetitive geometry of the Liver to probabilistically model variations in shape and geometry. Proper registration of training data is crucial for successful implementation [4].

Medical image segmentation is a critical method for visualizing and correlating the volumetric and shape characteristics of human Liver structures. Over time, various methods have been employed for segmenting Liver structures from MRI scans. One such method is the Gaussian Mixture Model (GMM), which has been shown to be highly effective in accurately describing the intensities of Liver MR images, as demonstrated by [5] In previous studies, [6-8] investigated the application of mixed Gaussian distributions in representing pixel/voxel intensities in specific regions of interest. [9] expanded on this approach by implementing GMM to categorize voxels as either vascular tissue or non-vascular tissue based on their likelihood density. The process of segmenting Liver arteries can be considered as a problem of estimating parameters, which can be tackled using various algorithms. One of the most notable algorithms is the EM algorithm, as discussed by [10]. [11] is a highly respected source in the field. Although EM systems are generally known for their high convergence rate, there are situations where proper convergence cannot be guaranteed. Tumours can appear in any location, size, shape, and intensity, making it a complex task to automatically segment them [12]. Therefore, a multidisciplinary approach is necessary to address the complexities associated with automatic Liver tumour segmentation. Automated segmentation routines that integrate advanced artificial intelligence systems were proposed by [13]. This system incorporates various layers of information, such as voxel intensities, auxiliary soundness, geographical areas, and user input.

In [14] and his team introduced a neuro-fuzzy segmentation approach for MRI data that could differentiate between different types of tissues, including WM, GM, CSF, and tumours. They utilized the K-Nearest Neighbour algorithm to merge multiple classifiers, resulting in the successful classification of Liver tissues. Additionally, Accurate identification and diagnosis of Liver tumours is crucial for medical professionals. However, the MRF approach, while effective, incurs a significant computational cost. To address this, the

clustering primary process is employed as a preliminary segmentation and approximation of MRF parameters. This information simplifies the identification and diagnosis of Liver tumours for medical professionals. [15] emphasized the importance of evaluating patients for accurate diagnosis. However, previous methods have been limited in their effectiveness. [16] have also presented an enhanced 2-D tumour segmentation method that employs partial differential equations to represent cerebral MRI images and an automated Liver tumour identification approach. Furthermore, a new procedure has been developed to remove the skull. The results of testing this innovative method on various Liver scans have demonstrated a high Peak Signal-to-Noise Ratio (PSNR), indicating its efficacy. The accurate identification of tumors through precision is of utmost importance. [17] developed a grouping method that uses switching and has been effectively utilized on MRI Liver images that contain salt and noise. The efficacy of this technique has been quantitatively assessed and confirmed.

The present study has successfully created non-linear diffusion filters that possess distinct boundaries. These filters were designed to distribute edges across different inclination scales and to minimize conservative noise. Additionally, [18] have introduced a new segmentation method that utilizes fuzzy anisotropic diffusion and grading. The Markov Random Field (MRF) is a mathematical concept that describes a random field exhibiting Markovian properties. Its effectiveness in addressing medical imaging issues has been demonstrated in the field of MRI Liver segmentation [19]. The Hidden Markov Random Field (HMRF) model is an extension of the MRF, which infers hidden states through an observation field. [20] introduced the use of MRF-based automatic Liver segmentation through atlas registration, utilizing simple techniques. This novel approach combines biological and medicinal treatments and relies on atlas registration. The Liver tumour being studied is classified as an MRF. An automated process can enhance the resolution of low-quality images by selecting appropriate photographs that highlight any irregularities and images of skull removal. This process utilizes a sequence of wavelets generated by an orthonormal series to represent an integrated square function, as described by [21]. After undergoing wavelet transformation, the grayscale image's diagonal, vertical, and horizontal coefficients are saved for further analysis. [22] developed the Wavelet transformation approach to facilitate segmentation, which can adapt to frequency, temporal, and image discontinuities. Furthermore, the morphology filtering technique was created to further enhance image quality. [23]devised a method to ascertain the size and shape of a structure's image by utilizing input and structural images. The effectiveness of this technique was tested on 50 patients with various types of tumours, and it demonstrated remarkable results. The Gaussian filtering method, developed by [24], aimed to eliminate unnecessary passages during the autumn and growth seasons. The modification of the function is also known as the Weierstrass transformation.

The Gaussian filter inputs undergo both discrete and continuous processing. In their study, [25] employed a combination of 2D-CWT and Incremental Supervised Neural Network (ISNN) to segment Liver images into seven distinct classes. There are a variety of techniques available for image segmentation, and the chosen method can greatly impact the overall efficacy of the approach. [26] introduced the skull stripping method to tackle the challenges of low-contrast images and inaccurate segmentation caused by MR scanner parameters in Liver tumor analysis. The analysis of images can be made more intricate than the use of clustering methods. [27] have discovered a dependable approach to normalizing intensity in image segmentation. They determined the mean and standard deviation of intensity values for each sequence and standardized them to have a mean of one and a variance of one. This method has been implemented in MRI image segmentation to improve image quality, intensity, and contrast for patients. [28] have also created GLCM textural features for identifying Liver tumors. The purpose of the detection approach is to identify tumours, and it has been developed and tested using MR images of simulated tumours. [29] introduced a new technique for segmenting Liver cell division, which is a crucial step in medical processing. The goal of this technique is to detect any abnormalities or debris present in the Liver. By using a progressive approach to the planting location, this technique improves the accuracy of locating the specific area of the Liver where the tumour is located. The benefit of using this method is that it effectively cleans up the real-world MRI data set, enabling clear and distinct pixel visualization. This technique proves to be particularly useful in identifying tumours. In [30] presented a state-of-the-art model for the detection of gliomas in the Liver, a type of tumor that originates from glial cells and is responsible for 80% of malignant diseases. [31] introduced a new active contour model, referred to as the river basin technique, which was utilized to map the tumour region in Liver tumour segmentation. Building on this work, [32] proposed a river basin segmentation method that utilizes connected component labelling coding to detect tumour segmentation. This study explores the potential of hydrographic segmentation, including image acquisition, image preprocessing, and contrast parameter. The Watershed technique is a useful tool for surgeons to differentiate between abnormal and normal tissue. This approach provides benefits such as simplicity, consistency, and reduced noise. Additionally, high-frequency MRI components can be extracted from MR images, which allows for precise calculations of various variables,

including location, shape, perimeter, eccentricity, entropy, and centroid. [33] introduced the Atlas deformation technique to address complex tumor regions. This approach involves three stages to describe the progression and current state of the lesion. [34] introduced a novel approach for identifying Liver tumours that is both automatic and unsupervised. This two-step strategy is founded on automated and intensity objectives and is entirely accessible. [35] have introduced systematic methods to validate the precision of automatic image segmentation, which has enabled the probabilistic classification of tumor types based on pixels. In [36], developed the Expectation Maximization (EM) algorithm to determine the latent gold standard. Additionally, they combined two beta distributions with different form factors to simulate the results of probability segmentation.

The main contributions of this work are summarized below:

A Multi-variate Multi-region tumor filtering for feature extraction process.

A Multi-variate Multi-region tumor feature extraction and segmentation on multi-variate multi-oriented arbitrary liver tumor regions for classification process.

A Multi-variate Liver and tumor segmentation and classification(MCMVLTSC) framework on heterogeneous tumor detection process.

2. Multi-Variate Liver and Tumor Segmentation and Classification (MCMVLTSC)

1. Multi-variate Liver data filtering

Liver image filtering plays a crucial role in the analysis of liver images, particularly in tasks such as feature selection, denoising, and compression. One commonly used technique is sparse filtering, which aims to remove sparse noise from the dataset. However, in some cases, a more flexible and expressive approach is required to capture the complex relationships and underlying structure of the data. This is where multi-variate non-linear Gaussian estimation (MNGE) comes into play. NGE is a powerful method for estimating the parameters of a non-linear Gaussian model. Unlike sparse filtering, which is a linear feature selection technique, NGE allows for non-linear relationships to be modeled effectively. By combining NGE with sparse filtering, it becomes possible to learn a non-linear Gaussian model that incorporates sparsity. The process of applying NGE and sparse filtering for liver image filtering involves several steps. First, the parameters of the non-linear Gaussian model are estimated using NGE. This estimation takes into account the non-linear relationships present in the liver images, allowing for a more accurate representation of the underlying data distribution. Once the non-linear Gaussian model is established, sparse filtering is applied to remove sparse noise from the liver image dataset. Sparse filtering selectively retains the most relevant and informative features while discarding the noise and irrelevant components. This step helps to improve the accuracy and relevance of the subsequent liver image analysis. It is important to note that the specific implementation of NGE and sparse filtering may vary depending on the characteristics of the liver image dataset and the desired outcome. Different variations of MNGE algorithms, such as variational Bayesian methods or expectation-maximization algorithms, can be employed to estimate the non-linear Gaussian parameters effectively. Similarly, various sparse filtering techniques, such as L1 regularization or sparse coding, can be utilized for noise removal. The combined use of NGE and sparse filtering offers a powerful approach for liver image filtering. By leveraging the flexibility of NGE to model non-linear relationships and the selective feature retention of sparse filtering, the accuracy and relevance of liver image analysis can be significantly improved. This method enables researchers and medical professionals to extract meaningful information from liver images, leading to enhanced diagnostic capabilities and improved understanding of liver diseases as shown in figure 2.

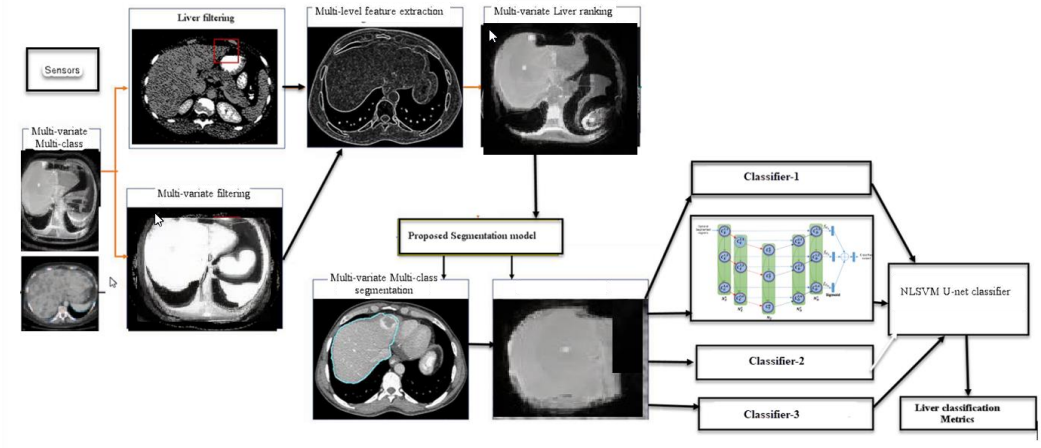

Fig. 2. Proposed Framework

In figure 2, each multi-variate image data are taken as input for the multi-variate filtering and multi-variate feature extraction process. Here different modalities of feature ranking measures are used to filter the essential key features for the multi-class multi-variate segmentaion approach. Finally, classification framework is used to optimize the multi-class tumor detection . To identify the sparse features in partitioned data with a high degree of missing values, which makes accurate predictions even with limited data, the proposed equation called Non-linear Gaussian estimation can be used.

Probabilistic GMM:

The GMM_nf(si, Θ_nf) represents the probability of a tumor's features (si) belonging to the GMM for non-fatty liver samples.It is computed by summing the weighted PDFs of each component in the GMM.Each component k is associated with a weight (w_nf,k), mean (μ_nf,k), and covariance (Σ_nf,k).

GenerateProbabilityMap Function:

1. The function takes the non-fatty liver samples as input and optimizes the GMM parameters (Θ_nf) using the optimizeGMMParameters function (using expectation maximization).

2. It initializes an empty 3D array called probabilityMap to store the probability values for each tumor.

3. For each tumor in the volume, it extracts the tumor's features using the extractFeatures function.

4. The calculateGMMProbability function is then used to calculate the probability (probability_nf) of the tumor features belonging to the GMM_nf.

5. The probability_nf value is assigned to the corresponding tumor in the probabilityMap.

6. Finally, the log likelihood estimation of each image is returned.

Liver image filtering is a process used to remove noise and irrelevant features from a dataset of liver images with numerical features. The goal of this process is to improve the accuracy of any analysis or modeling performed on the dataset. The filtering process involves several steps. First, for each numerical feature in the dataset, the NLG is calculated. Next, for each value in the dataset, the observed and expected frequency of the value is computed, and the chi-squared contribution of the value is calculated. The chi-squared statistic is then computed for the entire dataset. The mutual information between each feature and the dataset is also calculated. Based on the computed chi-squared statistic and mutual information, values with low scores are removed from the dataset. The remaining values form the filtered dataset, which can be used for further analysis or modelling. The specific implementation of this process may vary depending on the dataset and the desired outcome.

2.1 Multi-variate Feature extraction measures

a. Multi-variate Gaussian Mixture Model (GMM) features:

$GMM\_nf(si, \Theta\_nf) = \Sigma k=1 \text{ to } K\ w\_nf,k * N(si ; \mu\_nf,k, \Sigma\_nf,k)$

Optimization of GMM parameters (weights, means, and covariances) using expectation maximization:

$\Theta\_nf^* = \text{argmax}(\prod i=1 \text{ to } T\ GMM\_nf(si ; \Theta\_nf))$

o calculate the probability of a tumor's features belonging to a Gaussian Mixture Model (GMM), you can use the following steps:

Calculate the probability density function (PDF) for each component of the GMM.

For a given tumor feature vector x, the PDF of a component k can be calculated as:

$pdf\_k = N(x ; \mu\_k, \Sigma\_k)$

where $N(x ; \mu\_k, \Sigma\_k)$ is the multivariate normal distribution with mean vector μ_k and covariance matrix Σ_k.

Compute the weighted sum of the PDFs for all components of the GMM.

For a GMM with K components, the probability P of the block region features belonging to the GMM can be calculated as:

$P = \Sigma k=1 \text{ to } K\ w\_k * pdf\_k$

posterior_nf = P* (likelihood_nf * prior_nf) / ((likelihood_nf * prior_nf) + (likelihood_bnf * prior_bnf))

posterior_f = P (likelihood_f * prior_f) / ((likelihood_f * prior_f) + (likelihood_bf * prior_bf))

where w_k is the weight associated with component k.

b. Generative probabilistic map features:

```
function generateProbabilityMap(nonFattySamples):
    Θ_nf = optimizeGMMParameters(nonFattySamples)
    probabilityMap = empty 3D array
        for each tumor in volume:
        tumorFeatures = extractFeatures(tumor) // Extract features of the tumor
        probability_nf = calculateGMMProbability(tumorFeatures, Θ_nf) // Using GMM_nf
        probabilityMap[tumor] = probability_nf
    return probabilityMap
```

```
function calculateGMMProbability(features, Θ):
    probability = 0
    for each component k in Θ:
        weight = Θ.weight[k]
        mean = Θ.mean[k]
        covariance = Θ.covariance[k]
        pdf = calculateMultivariateNormalPDF(features, mean, covariance)
        probability += weight * pdf
    return probability
```

c. Block wise NLM features

The traditional non-local means algorithm (NLM) can yield poor results due to its non-locality of neighboring pixels.To address this, a block-based NLM method is proposed, which significantly reduces computational time.

The block-based approach helps reduce the computational cost by performing the NLM restoration on blocks instead of individual pixels. The block-based non-local means algorithm enhances the traditional NLM method by considering blocks instead of pixels, using overlapping constraints, and averaging approximations. By applying NLM restoration on blocks, it improves the denoising process and reduces computational time, making it more efficient for tumor feature extraction in biomedical images.

3. Multi-Variate Feature Ranking Algorithm

Multi-variate joint probabilistic feature extraction techniques play a vital role in liver image segmentation processes, enabling the identification and segmentation of liver tissue. These methods utilize probabilistic models to extract relevant features from liver images, aiding in accurate segmentation.One prominent approach to probabilistic feature extraction in liver image segmentation is the Hidden Markov Model (HMM). The HMM represents a liver image as a sequence of hidden states and observed features. The hidden states capture the underlying structure of the liver image, while the observed features correspond to the actual pixel values. By calculating the probability distribution of the hidden states given the observed features, the HMM facilitates the segmentation of the liver tissue into distinct segments.Another method is the use of theta regulated Gaussian Mixture Models (TGMMs). TGMMs represent the liver image as a combination of Gaussian distributions, where each distribution represents a specific type of liver tissue. The model calculates the probability distribution of the liver image given the observed features and utilizes this information to segment the liver tissue accurately.Additionally, the theta control Markov Random Field (TMRF) model is employed for probabilistic feature extraction in liver image segmentation. This model treats the liver image as a graph, with individual pixels acting as nodes and the edges representing the spatial relationships between pixels. The TMRF model establishes a prior distribution and a likelihood function to calculate the probability distribution of the liver image given the observed features. The prior distribution incorporates statistical characteristics and the spatial layout of the liver tissue, while the likelihood function assesses the conformity of the observed features to the prior distribution. Combining the prior distribution and likelihood function enables the TMRF model to accurately calculate the probability distribution of the liver image, facilitating precise segmentation of the liver tissue.These probabilistic feature extraction methods are valuable tools in liver image segmentation, aiding in the identification and segmentation of liver tissue. By leveraging probabilistic models and their associated probability distributions, these techniques.

4. Weighted Joint Probabilistic Liver Segmentation Approach

The K-Density probabilistic segmentation approach estimates the probability density function of each liver tissue cluster using a kernel density estimator. This approach has several benefits when handling imbalanced liver datasets. It can handle liver images with a significant degree of class imbalance, where the minority class has a very low sample size, and can withstand image noise and outliers. The K-Density probabilistic clustering approach can locate complex and non-linear liver tissue clusters, which is crucial for numerous real-world applications.One of the main benefits of the K-Density probabilistic clustering approach is its ability to be applied to both binary and multi-class liver segmentation issues. It can also be utilized for unsupervised learning when the number of liver tissue classes is unknown in advance. Another benefit of the K-Density probabilistic clustering approach is its ability to be used with other methods to enhance the performance of liver image segmentation models. Liver automatic segmentation using joint probability estimations involves finding the optimal segmentation of liver images by estimating the joint probability distribution of the data. The inputs to the algorithm include a filtered Imbalanced liver dataset and the number of segmentation regions K.The first step is to initialize the mixture model by randomly assigning parameters to K Gaussian mixture components. The Expectation step involves calculating the posterior probability of each region belonging to each of the K segmentation regions using Bayes' theorem. The Maximization step involves updating the parameters of each mixture component by calculating the mean, covariance matrix, and prior probability using the posterior probabilities calculated in the Expectation step. These steps are repeated until convergence is obtained, which is

checked by monitoring the change in the log-likelihood of the data. If the log-likelihood does not change significantly, the algorithm stops and returns the final segmentation vector, which indicates the segmentation assignment for each region.The algorithm calculates the probability of selecting each segmentation region score based on its density using the joint probability distribution of the data. This approach can accurately segment the liver tissue even in the presence of imbalanced liver datasets and can locate complex and non-linear segmentation regions.

Output the estimated parameters of the multimodal distribution: the mixing weights (π_k) and the parameters of each component distribution (θ_k). The steps involve computing responsibilities based on the current parameter estimates, updating the parameters in the M-step using the responsibilities, and repeating the joint estimation JE-step and joint maximization JM-step until convergence is achieved. The algorithm aims to maximize the likelihood function or the log-likelihood function to estimate the parameters of the multimodal distribution.

5. Multi-Variate Multi-Level Boosting Classifier

5.1 Proposed NL-SVM U-Net Model

The U-Net architecture is a widely used deep learning model that has proven to be effective for image segmentation tasks, including tumor detection. It derives its name from its U-shaped structure, which comprises an encoding path and a decoding path.In the encoding path, the input signal undergoes a series of operations within each layer. Firstly, the input is convolved with learnable filters represented by weights (w_l) and a bias term (b_l). This convolution operation allows the network to capture local patterns and features present in the input signal. An activation function (f_l) is then applied to introduce non-linearity, enabling the model to learn complex relationships in the data. The output of this activation function is stored as (c_l). Additionally, a pooling operation with a specified size (p_l) and stride (s_l) is performed to down-sample the signal, reducing its spatial dimensions while preserving important features as shown in figure 3.

In the decoding path, the down-sampled signal (c_l) is fed through a series of layers that perform the reverse operations of the encoding path. An up-sampling operation is applied to increase the spatial dimensions of the signal, effectively reconstructing its original resolution. This up-sampled signal is then convolved with filters (w_u) to capture fine-grained details and activate relevant features. An activation function (f_u) is subsequently applied, and the output is stored as (c_ul).

Define each network layer variables:
For layer l in the network:
Pass the input signal c_l-1 through the encoding path:
Apply a convolution operation with weight w_l and bias b_l
Apply an activation function f_l
Store the output in c_l
Apply a pooling operation with size p_l and stride s_l to down-sample the signal
Pass the down-sampled signal c_l through the decoding path:
Apply an up-sampling operation to c_l using the deconvolution layer with weight w_u and bias b_u
Apply an activation function f_u
Store the output in c_ul
Apply a residual operation to c_l-1 and c_ul using the residual block with weight theta_u
Store the output in c_ul_hat
Apply a convolution operation to c_l-1 - c_ul using the convolution layer with weight w_s and bias b_s
Apply an activation function f_s
Store the output in c_st
Apply a residual operation to c_l-1 - c_ul and c_st using the residual block with weight theta_s
Store the output in c_s_hat
Combine the output of the up-sampling and shortcut paths to form p_prop:
If the object size is large:
Apply a residual operation to c_l-1 and c_low_l-1 using the residual block with weight theta_s
Apply an up-sampling operation to c_l-1 - c_low_l-1 using the deconvolution layer with weight w_u and bias b_u
Store the output in c_ul
Set c_ul_hat to c_low_l-1
Else if the object size is small:
Set c_ul and c_ul_hat to 0
Apply an up-sampling operation to c_l using the deconvolution layer with weight w_u and bias b_u
Apply an activation function f_u

Store the output in c_ul

Combine c_s_hat and c_ul using an element-wise sum

Combine the sum with the output of the up-sampling operation to form p_prop:

Apply an activation function f_prop

Store the output in c_l+1

For each feature set do

$$min_{W_k,a_k}\ \frac{1}{2}\|W_k\|_1^2 + \tau_m + sig(i)\,.\sum_{i=1}^{l} a_i(y_i[ker\langle x,y\rangle.w+b]1+\xi_i) - \sum_{i=1}^{l}\gamma_i\xi_i \qquad (6)$$

$$s.t\ sig(i)\,.ker\langle x,y\rangle.w+b\ \geq 1-\xi_i^n-\ \tau_m$$

$$\xi_i^n > 0, \qquad \tau_m > 0;\ \ m = 1 \ldots\ldots classes$$

Here kernel function $\ker\langle x,y\rangle$ represents the kernel functions defined from C3D features space to classes.

$$\ker\langle x,y\rangle = \begin{cases} e^{-sig(i)\,.\xi_i^n \log(\sum\|x-y\|^2} & if\ x=y \\ e^{-sig(i)\,.\xi_i^n \log(\sum\|x-y\|^{\frac{1}{2}}} & if\ x<y \\ e^{-sig(i)\,.\xi_i^n \log(\sum\|y\|^2} & if\ x>y \end{cases}$$

$$sig(i) = \frac{m_{inp}^{(mx)}}{1+e(-\lambda(i-\phi))}$$

$$\phi = \frac{1}{2}(m_{inp}^{(mx)} - m_{inp}^{(mn)})$$

$m_{inp}^{(mx)}$: *mean* value of maximum likelyhood function in the input image inp.

$m_{inp}^{(mn)}$: *mean* value of minimum likelyhood function in the input image inp.

λ : *scaling* factor.

Return the final output signal from the topmost decoder layer (i.e., p_prop of the last layer).

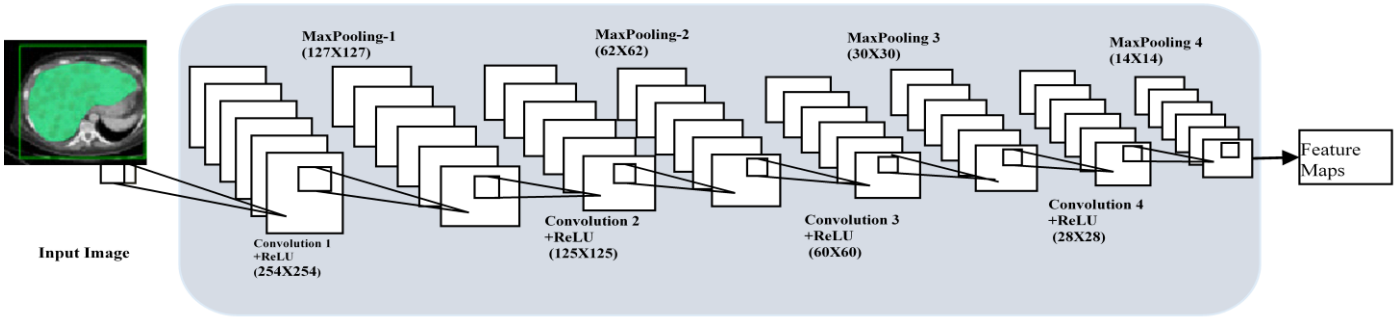

Fig.3. U-net MSVM features

A residual operation is then performed, combining the information from the corresponding encoding layer (c_l-1) and the current decoding layer (c_ul) using a residual block with learnable weights (theta_u). The output is stored as (c_ul_hat). Furthermore, a convolution operation is applied to the difference between (c_l-1) and (c_ul) using weights (w_s) and a bias term (b_s), followed by an activation function (f_s). The output is stored as (c_st). Another residual operation is performed to combine the information from (c_l-1) - (c_ul) and (c_st) using a residual block with learnable weights (theta_s), and the output is stored as (c_s_hat).To form the p_prop, which represents the combined output of the up-sampling and shortcut paths, the following steps are taken based on the object size:

If the object size is large, a residual operation is applied to (c_l-1) and (c_low_l-1) using a residual block with weights (theta_s). An up-sampling operation is then performed on (c_l-1) - (c_low_l-1) using the deconvolution layer with weights (w_u) and a bias term (b_u), and the output is stored as (c_ul). (c_ul_hat) is set equal to (c_low_l-1).

If the object size is small, (c_ul) and (c_ul_hat) are both set to 0. An up-sampling operation is applied to (c_l) using the deconvolution layer with weights (w_u) and a bias term (b_u), and an activation function (f_u) is applied. The output is stored as (c_ul).The outputs (c_s_hat) and (c_ul)

are combined using an element-wise sum, and the sum is further combined with the output of the up-sampling operation. An activation function (f_prop) is applied to the final result, which is then stored as (c_l+1).

Additionally, for each feature set, an optimization problem is solved, where the goal is to minimize a cost function given by Equation (6). The variables in the optimization problem include the weights (W_k) and the parameters (a_k). The main problem aims to balance the regularization term, the classification term, and the error term. The regularization term is represented by 1/2 ‖W_k ‖_1^2, promoting sparse and compact representations. The classification term involves the weighted sum of activation values (a_i) multiplied by the predicted outputs (y_i) obtained by convolving the kernel function (ker⟨x,y⟩) with the weights (w) and adding the bias term (b). This term encourages the network to classify the input correctly. The error term involves the weighted sum of slack variables (ξ_i), penalizing misclassifications and deviations from the desired margin.The optimization problem is subject to constraints, where ker⟨x,y⟩.w+b should be greater than or equal to 1 minus ξ_i^n- τ_m. Here, ξ_i^n represents the non-negative slack variables, and τ_m represents a positive threshold specific to each class. These constraints ensure that the classification score for the correct class is greater than the scores for other classes by a certain margin.The kernel function, ker⟨x,y⟩, is defined based on the C3D feature space and is responsible for mapping the features to the corresponding classes. It employs different formulations depending on the relative magnitudes of x and y. If x and y are equal, the kernel function employs the squared Euclidean distance between x and y. If x is smaller than y, it employs the square root of the Euclidean distance. And if x is greater than y, it only considers the Euclidean distance of y. These different formulations of the kernel function enable the model to handle varying feature magnitudes and distances.Finally, the output signal from the topmost decoder layer, p_prop, represents the final segmentation output of the U-Net model. It encapsulates the segmented tumor regions obtained through the entire encoding and decoding process. This output can be utilized for further analysis, visualization, or clinical decision-making.

6. Experimental Analysis

In this section, the proposed framework and its experimental findings are presented, evaluating the precision, accuracy, recall, and F-measure. Diverse imbalanced datasets were used for classification tasks, and liver segmentation stage. In these experiments, a large collection of CT images was used, consisting of both healthy liver images and images of liver cancer. In these experiments, a large collection of CT images was used, consisting of both healthy liver images and images of liver cancer. A total of 600 clinically acquired CT images were obtained, with 300 depicting hepatocellular carcinoma (HCC) and 300 depicting metastatic liver tumors (MET). A region of interest (ROI) measuring 30 x 30 pixels was extracted from each image.For each image, a single ROI was calculated. The typical ROI could be chosen from the entire liver area, while the ROI representing the tumor could be chosen from the abnormal liver regions affected by HCC or MET. The input for tumor detection could be selected from the collection of all images. Once the tumors were detected, the aberrant liver regions affected by HCC (primary liver cancer) and MET (secondary liver cancer) were used as inputs. An appropriate tumor region was then extracted as an ROI from each of these images.The ROI from each image was used to select the input ROI (IROI). While a certain image had only one selected ROI, the IROI could vary from 1 to 5 depending on the intended performance. The division of data into training and testing sets was determined based on the desired performance. To address this, two web databases were downloaded and utilized: the LiTS database, which included 131 3D CT scans collected from 6 medical facilities (with evaluation focused on the training component), and the 3D-IRCADb-01 database, which included 3D CT scans of 10 women and 10 men with hepatic tumors in 75% of instances. These datasets encompassed primary and secondary liver tumors and metastases, and they were acquired using various scanners and scanning techniques. Each of the approximately 2,800 slices in the DICOM format contained masks for the liver, tumors, bones, arteries, kidneys, and lungs. This dataset was suitable for use with CNN models and was recommended in a previous research work [20].

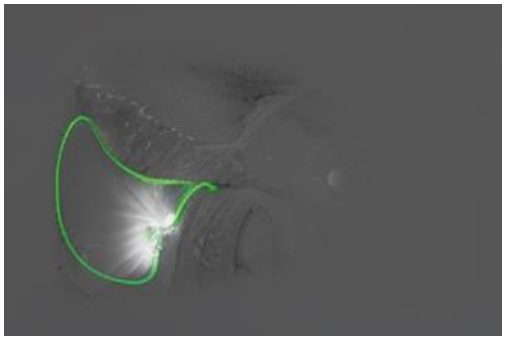

Fig. 4. Liver tumor automatic detecditon with variable size

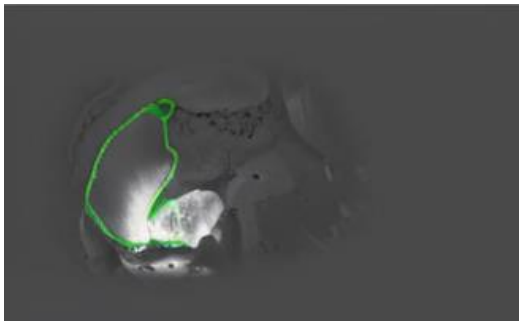

Fig. 5. Automatic liver tumor detection with different orientation and shape

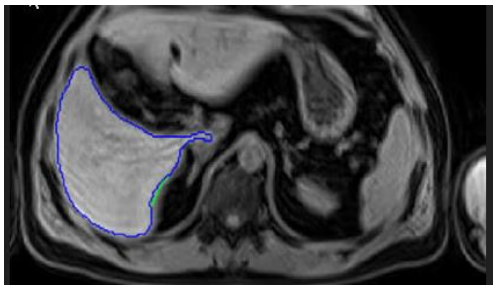

Fig. 6. Automatic liver tumor detection with proposed multi-variate segmentation based classification approach

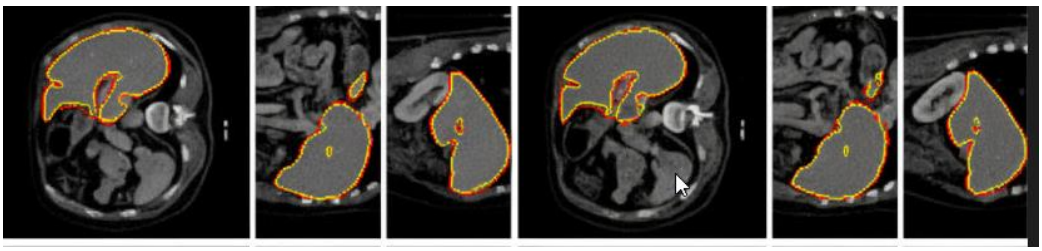

Fig. 7. Automatic liver tumor detection with proposed multi-variate segmentation based classification approach

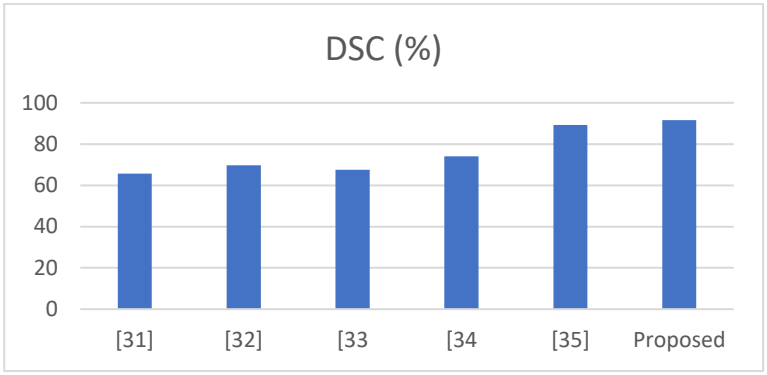

Fig. 8. Comparison of Dice similarity Coefficient of different existing models to the proposed model.

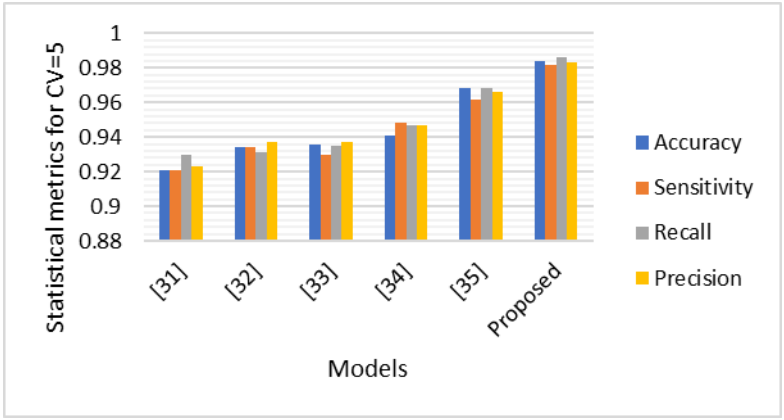

Fig. 9. Compartive analysis of proposed multi-variate multi-class tumor detection to the conventional approaches.(Cross validation 5)

Table 1. Compartive analysis of proposed multi-variate multi-class tumor detection to the conventional approaches.

Liver heterogeneous DB CV=10						
Accuracy	0.93	0.934	0.939	0.942	0.964	0.981
Sensitivity	0.938	0.937	0.932	0.942	0.964	0.987
Recall	0.936	0.936	0.932	0.943	0.96	0.985

Precision	0.924	0.938	0.939	0.948	0.961	0.987
Runtime(ms)	3404	3280	3232	3147	3010	2718

The given metrics for liver tumor detection include Accuracy, Sensitivity, Recall, Precision, and Runtime (in milliseconds) for a liver heterogeneous database with cross-validation (CV=10).

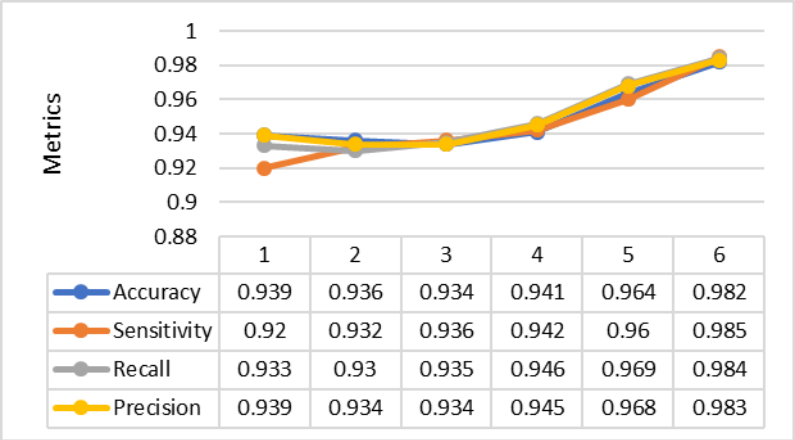

Fig.10. Compartive analysis of proposed multi-variate multi-class tumor detection to the conventional approaches. (Cross validation 15)

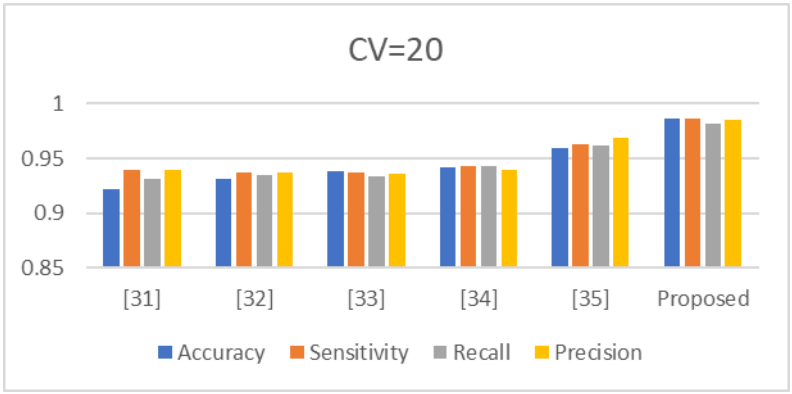

Fig. 11. Compartive analysis of proposed multi-variate multi-class tumor detection to the conventional approaches. (Cross validation 5)

Table 2. represents metrics for liver tumor detection are Accuracy, Sensitivity, Recall, Precision, and Runtime (in milliseconds).

Metrics	**[31]**	**[32]**	**[33]**	**[34]**	**[35]**	**Proposed**
Accuracy	0.933	0.931	0.931	0.947	0.965	0.982
Sensitivity	0.936	0.931	0.936	0.942	0.961	0.988
Recall	0.935	0.936	0.931	0.948	0.966	0.981
Precision	0.922	0.934	0.932	0.942	0.96	0.985
Runtime(ms)	3382	3293	3224	3180	3025	2714

7. Conclusion

In conclusion, this research paper introduces an automatic multivariate multi-class feature extraction, ranking based joint probabilistic segmentation and classification framework for multi-class liver tumor detection. The study addresses the challenges faced by existing liver segmentation models, including multi-modal tumor detection, variation in tumor shapes, liver over-segmentation, and difficulty in identifying tumors with diverse orientations and shapes. The presence of noise in excessively segmented border regions further complicates the segmentation and classification process, leading to inconsistent and inaccurate results.To overcome these challenges, the paper proposes novel approaches for multivariate liver filtering, multivariate feature extraction, and ranking. These techniques improve the overall detection of multi-modal tumors on large databases. The proposed Multi-variate Liver and Tumor Segmentation and Classification (MCMVLTSC) model efficiently classifies

key tumor segmented regions with a high true positive rate and runtime efficiency (ms).To evaluate the performance of the MCMVLTSC model, various statistical measures are utilized on diverse liver imaging databases. Experimental results demonstrate that the proposed model surpasses conventional models in terms of different statistical classification metrics and runtime efficiency.The findings of this study highlight the potential of the proposed framework for accurate and efficient multi-class liver tumor detection. By integrating multivariate feature extraction, ranking, and joint probabilistic segmentation and classification, the model addresses the limitations of existing approaches. This research contributes to the field of liver disease diagnosis and treatment by providing a robust and reliable tool for automatic tumor detection in large heterogeneous liver databases.

Authors Contribution: Authors contributed equally to this work.

Data Availability: Not applicable

Declarations

Ethics Approval: Not applicable.

Consent to Participate: Not applicable.

Consent for Publication: Not applicable.

Conflict of interest: No competing interests.

References

[1] P. Lv, J. Wang, and H. Wang, "2.5D lightweight RIU-Net for automatic liver and tumor segmentation from CT," Biomedical Signal Processing and Control, vol. 75, p. 103567, May 2022, doi: 10.1016/j.bspc.2022.103567.

[2] R. Rong et al., "A Deep Learning Approach for Histology-Based Nucleus Segmentation and Tumor Microenvironment Characterization," Modern Pathology, vol. 36, no. 8, p. 100196, Aug. 2023, doi: 10.1016/j.modpat.2023.100196.

[3] N. N. Prakash, V. Rajesh, D. L. Namakhwa, S. Dwarkanath Pande, and S. H. Ahammad, "A DenseNet CNN-based liver lesion prediction and classification for future medical diagnosis," Scientific African, vol. 20, p. e01629, Jul. 2023, doi: 10.1016/j.sciaf.2023.e01629.

[4] R. Wu, Y. Xin, J. Qian, and Y. Dong, "A multi-scale interactive U-Net for pulmonary vessel segmentation method based on transfer learning," Biomedical Signal Processing and Control, vol. 80, p. 104407, Feb. 2023, doi: 10.1016/j.bspc.2022.104407.

[5] C. Dong, S. Xu, D. Dai, Y. Zhang, C. Zhang, and Z. Li, "A novel multi-attention, multi-scale 3D deep network for coronary artery segmentation," Medical Image Analysis, vol. 85, p. 102745, Apr. 2023, doi: 10.1016/j.media.2023.102745.

[6] Y. Fu, Y. Lei, T. Wang, W. J. Curran, T. Liu, and X. Yang, "A review of deep learning based methods for medical image multi-organ segmentation," Physica Medica, vol. 85, pp. 107–122, May 2021, doi: 10.1016/j.ejmp.2021.05.003.

[7] H. Jiang et al., "A review of deep learning-based multiple-lesion recognition from medical images: classification, detection and segmentation," Computers in Biology and Medicine, vol. 157, p. 106726, May 2023, doi: 10.1016/j.compbiomed.2023.106726.

[8] P.-H. Conze et al., "Abdominal multi-organ segmentation with cascaded convolutional and adversarial deep networks," Artificial Intelligence in Medicine, vol. 117, p. 102109, Jul. 2021, doi: 10.1016/j.artmed.2021.102109.

[9] V. Czipczer and A. Manno-Kovacs, "Adaptable volumetric liver segmentation model for CT images using region-based features and convolutional neural network," Neurocomputing, vol. 505, pp. 388–401, Sep. 2022, doi: 10.1016/j.neucom.2022.07.024.

[10] S. Liu, H. Wang, Y. Li, X. Li, G. Cao, and W. Cao, "AHU-MultiNet: Adaptive loss balancing based on homoscedastic uncertainty in multi-task medical image segmentation network," Computers in Biology and Medicine, vol. 150, p. 106157, Nov. 2022.

[11] G. M. Dogar, M. Shahzad, and M. M. Fraz, "Attention augmented distance regression and classification network for nuclei instance segmentation and type classification in histology images," Biomedical Signal Processing and Control, vol. 79, p. 104199, Jan. 2023, doi: 10.1016/j.bspc.2022.104199.

[12] M. Wang, R. Jin, J. Lu, E. Song, and G. Ma, "Automatic CT liver Couinaud segmentation based on key bifurcation detection with attentive residual hourglass-based cascaded network," Computers in Biology and Medicine, vol. 144, p. 105363, May 2022.

[13] S. Di, Y. Zhao, M. Liao, Z. Yang, and Y. Zeng, "Automatic liver tumor segmentation from CT images using hierarchical iterative superpixels and local statistical features," Expert Systems with Applications, vol. 203, p. 117347, Oct. 2022, doi: 10.1016/j.eswa.2022.117347.

[14] J. J. Sáenz-Gamboa, J. Domenech, A. Alonso-Manjarrés, J. A. Gómez, and M. de la Iglesia-Vayá, "Automatic semantic segmentation of the lumbar spine: Clinical applicability in a multi-parametric and multi-center study on magnetic resonance images," Artificial Intelligence in Medicine, vol. 140, p. 102559, Jun. 2023.

[15] Y. Ren, D. Zou, W. Xu, X. Zhao, W. Lu, and X. He, "Bimodal segmentation and classification of endoscopic ultrasonography images for solid

pancreatic tumor," Biomedical Signal Processing and Control, vol. 83, p. 104591, May 2023, doi: 10.1016/j.bspc.2023.104591.

[16] H. Gao, M. Lyu, X. Zhao, F. Yang, and X. Bai, "Contour-aware network with class-wise convolutions for 3D abdominal multi-organ segmentation," Medical Image Analysis, vol. 87, p. 102838, Jul. 2023, doi: 10.1016/j.media.2023.102838.

[17] Reddy, A. P. C., Kumar, M. S., Krishna, B. M., Inthiyaz, S., & Ahammad, S. H. (2019). Physical unclonable function based design for customized digital logic circuit. International Journal of Advanced Science and Technology, 28(8), 206-221.

[18] S. Gul, M. S. Khan, A. Bibi, A. Khandakar, M. A. Ayari, and M. E. H. Chowdhury, "Deep learning techniques for liver and liver tumor segmentation: A review," Computers in Biology and Medicine, vol. 147, p. 105620, Aug. 2022, doi: 10.1016/j.compbiomed.2022.105620.

[19] X. Zhong, H. Zhang, G. Li, and D. Ji, "Do you need sharpened details? Asking MMDC-Net: Multi-layer multi-scale dilated convolution network for retinal vessel segmentation," Computers in Biology and Medicine, vol. 150, p. 106198, Nov. 2022, doi: 10.1016/j.compbiomed.2022.106198.

[20] Y. Liu et al., "Double-branch U-Net for multi-scale organ segmentation," Methods, vol. 205, pp. 220–225, Sep. 2022, doi: 10.1016/j.ymeth.2022.07.002.

[21] V. Nainamalai et al., "Evaluation of clinical applicability of automated liver parenchyma segmentation of multi-center magnetic resonance images," European Journal of Radiology Open, vol. 9, p. 100448, Jan. 2022, doi: 10.1016/j.ejro.2022.100448.

[22] Rashed, Ahmed Nabih Zaki, SK Hasane Ahammad, Malek G. Daher, Vishal Sorathiya, Abrar Siddique, Sayed Asaduzzaman, Hasin Rehana et al. "Spatial single mode laser source interaction with measured pulse based parabolic index multimode fiber." Journal of Optical Communications.

[23] H. Liu et al., "GCHA-Net: Global context and hybrid attention network for automatic liver segmentation," Computers in Biology and Medicine, vol. 152, p. 106352, Jan. 2023, doi: 10.1016/j.compbiomed.2022.106352.

[24] Daher, M. G., Trabelsi, Y., Ahmed, N. M., Prajapati, Y. K., Sorathiya, V., Ahammad, S. H., ... & Rashed, A. N. Z. (2022). Detection of basal cancer cells using photodetector based on a novel surface plasmon resonance nanostructure employing perovskite layer with an ultra high sensitivity. Plasmonics, 17(6), 2365-2373.

[25] S. Graham et al., "Hover-Net: Simultaneous segmentation and classification of nuclei in multi-tissue histology images," Medical Image Analysis, vol. 58, p. 101563, Dec. 2019, doi: 10.1016/j.media.2019.101563.

[26] M. Byra et al., "Joint segmentation and classification of breast masses based on ultrasound radio-frequency data and convolutional neural networks," Ultrasonics, vol. 121, p. 106682, Apr. 2022, doi: 10.1016/j.ultras.2021.106682.

[27] Z. Diao, H. Jiang, and Y. Zhou, "Leverage prior texture information in deep learning-based liver tumor segmentation: A plug-and-play Texture-Based Auto Pseudo Label module," Computerized Medical Imaging and Graphics, vol. 106, p. 102217, Jun. 2023.

[28] T. Kushnure, S. Tyagi, and S. N. Talbar, "LiM-Net: Lightweight multi-level multiscale network with deep residual learning for automatic liver segmentation in CT images," Biomedical Signal Processing and Control, vol. 80, p. 104305, Feb. 2023, doi: 10.1016/j.bspc.2022.104305.

[29] H. Haseljić et al., "Liver segmentation using Turbolift learning for CT and cone-beam C-arm perfusion imaging," Computers in Biology and Medicine, vol. 154, p. 106539, Mar. 2023, doi: 10.1016/j.compbiomed.2023.106539.

[30] Zuhayer, A., Abd-Elnaby, M., Ahammad, S. H., Eid, M. M., Sorathiya, V., & Rashed, A. N. Z. (2022). A Gold-Plated Twin Core D-Formed Photonic Crystal Fiber (PCF) for Ultrahigh Sensitive Applications Based on Surface Plasmon Resonance (SPR) Approach. Plasmonics, 17(5), 2089-2101.

[31] H. Zhang, J. Liu, Z. Yu, and P. Wang, "MASG-GAN: A multi-view attention superpixel-guided generative adversarial network for efficient and simultaneous histopathology image segmentation and classification," Neurocomputing, vol. 463, pp. 275–291, Nov. 2021, doi: 10.1016/j.neucom.2021.08.039.

[32] Y. Liu, Y. Zhu, Y. Xin, Y. Zhang, D. Yang, and T. Xu, "MESTrans: Multi-scale embedding spatial transformer for medical image segmentation," Computer Methods and Programs in Biomedicine, vol. 233, p. 107493, May 2023, doi: 10.1016/j.cmpb.2023.107493.

[33] Q. Hao, S. Tian, L. Yu, and J. Wang, "MFUnetr: A transformer-based multi-task learning network for multi-organ segmentation from partially labeled datasets," Biomedical Signal Processing and Control, vol. 85, p. 105081, Aug. 2023, doi: 10.1016/j.bspc.2023.105081.

[34] D. T. Kushnure and S. N. Talbar, "MS-UNet: A multi-scale UNet with feature recalibration approach for automatic liver and tumor segmentation in CT images," Computerized Medical Imaging and Graphics, vol. 89, p. 101885, Apr. 2021, doi: 10.1016/j.compmedimag.2021.101885.

[35] X. Zhang, N. Jia, and Y. Wang, “Multi-input dense convolutional network for classification of hepatocellular carcinoma and intrahepatic cholangiocarcinoma,” Biomedical Signal Processing and Control, vol. 80, p. 104226, Feb. 2023, doi: 10.1016/j.bspc.2022.104226.

[36] N. Shen et al., “Multi-organ segmentation network for abdominal CT images based on spatial attention and deformable convolution,” Expert Systems with Applications, vol. 211, p. 118625, Jan. 2023, doi: 10.1016/j.eswa.2022.118625.